Remote Sensing'96, Spiteri (ed.) © 1997 Balkema, Rotterdam. ISBN 90 5410 855 X

Wavelet-based digital elevation model analysis

Mihai Datcu
Deutsche Forschungsanstalt für Luft- und Raumfahrt e.V. (DLR), Deutsches Fernerkundungsdatenzentrum (DFD), Wessling, Germany

Dragoş Luca & Klaus Seidel
Image Science Division, Communication Technology Laboratory, ETHZ, Zürich, Switzerland

ABSTRACT: Estimations of the local roughness of Digital Elevation Models (DEMs) have been used both for a better geological understanding of terrain structures and for a more accurate DEM interpolation leading to higher resolution terrain maps. This work investigates two fractal dimension estimators for the characterization of the roughness of DEMs: the power spectrum estimator and the wavelet-based estimator. The performance of these methods is compared in terms of image segmentation capabilities. Since wavelets and fractals are related by the same multiresolution concept, we expect to have better results using the wavelet analysis method. This expectation is confirmed by experiments on synthetic images and real DEMs: measurements of fractal parameters using wavelet-based methods are more reliable than the same measurements performed using other methods. Finally we discuss some examples in which the fractal analysis of DEMs allows the separation of different roughness classes and reveals artifacts in the computation of elevation data.

1 INTRODUCTION

Digital Elevation Models (DEMs) have become an important tool in many remote sensing applications like e.g. SAR simulators, orthorectification of satellite and airborne images, classification of ground cover types, Geographic Information Systems, etc. Still in most of the cases, the resolution of the available DEMs is unsufficient for the requirements of the corresponding applications. SAR interferometry allows the achievement of much better resolutions, however this technique is not yet available on a large scale and the resulting surface is affected by typical artifacts. In many applications high resolution DEMs are still obtained by interpolation of existing low resolution elevation data using some smoothing (e.g. spline) functions. The method is very simple but yields unsatisfactory results, since the smoothness of the resulting DEM is mainly determined by the interpolation and is usually higher than the smoothness of the corresponding terrain.

Relying on the observation that relief conserves the same statistical characteristics over a wide range of scales, other interpolation techniques have been developed that perform a multiresolution analysis of the elevation data. These techniques use fractal models to measure the local roughness of the DEM and to interpolate terrain more realistically according to the estimated roughness (Yokoya and Yamamoto, 1989; Polidori et al., 1991; Franceschetti et al., 1994). Fractal analysis is thus the first step in the computation of higher resolution DEMs and has also been applied to get a better understanding of the geological and geomorphic processes or to develop better models of topographic relief (Huang and Turcotte, 1990; Clarke, 1988; Clarke and Schweizer, 1991).

This work investigates two fractal dimension estimators for the characterization of DEMs: the power spectrum estimator and the wavelet-based estimator. The power spectrum method was selected as a reference since it has often been designated to be the algorithm which achieves the best performance (Stewart et al., 1993; Schepers et al., 1992). Our approach concentrates on the wavelet-based method and is motivated by the fact that wavelets and fractals are closely related by the concept of scale and share many common properties (Akujuobi and Baraniecki, 1994). We compare the two methods both on synthetic and on real elevation data. The result of this comparison shows that the wavelet-based estimator achieves a better reliability of the measurements in terms of their standard deviation and is better suited to the segmentation of fractal images.

The paper is organized as follows. Section 2 gives an overwiev of the fractal and wavelet theory emphasizing the common concept of scale. Section 3 presents the results of a comparison between the spectral and the wavelet-based fractal estimators based on synthetic images. This comparison is performed in terms of image segmentation capabilities, i.e. the al-

gorithms are applied to image windows of small size and the obtained set of measurements is analysed statistically. In the last section we discuss some examples in which the fractal analysis of DEMs allows the separation of different roughness classes and reveals artifacts in the computation of elevation data.

2 ELEMENTS OF FRACTAL AND WAVELET THEORY

Fractals are mathematical objects that show the same structure when examined at all possible scales (Mandelbrot, 1982). Although more formal definitions can be given, this qualitative characterization expresses the very essence of the fractal phenomenon and at the same time represents the basis for all fractal analysis algorithms: the algorithms check for fractal behaviour simply by examining the object at several scales (resolutions). The basic parameter characterizing a fractal object is its dimension: while non-fractal objects have dimensions given by integers (1 for curves, 2 for surfaces, etc.), fractals will have fractional dimensions since they represent transition structures between curves and surfaces, surfaces and solid bodies, etc.

The statistics of roughness measurements has been shown to agree – in a limited resolution range – with that of specific fractal models and several attempts have been made to characterize DEMs by means of the fractal theory. The most popular model used in this respect is the *fractional Brownian model (fBm)* (Voss, 1988). This model describes a signal $B_H(t)$ characterized by the fact that its increments between two moments of time t_1 and t_2 have a variance proportional to a power of the time lag $|t_2 - t_1|$:

$$E[|(B_H(t_2) - B_H(t_1)|^2] \propto |t_2 - t_1|^{2H} \quad (1)$$

Parameter H is called "Hurst exponent" ($0 < H < 1$) and is related to the dimension D of the corresponding fractal by (Voss, 1988):

$$D = n + 1 - H, \quad (2)$$

n being the topological dimension of the space in which the fractal object is represented ($n = 1$ for *fBm* time-functions, $n = 2$ for *fBm* surfaces, etc.). D will typically measure the "roughness" of the signal and most fractal analysis algorithms concentrate on an accurate estimation of D.

An analytical expression for fractional Brownian motion can be found in (Mandelbrot and van Ness, 1968) and (Wornell, 1993). From this expression, the autocorrelation function of fractional Brownian motion can be derived:

$$\begin{aligned} R_{B_H}(t,s) &= E\left[B_H(t)B_H(s)\right] \\ &= \frac{\sigma_H^2}{2}\left(|s|^{2H} + |t|^{2H} - |t-s|^{2H}\right) \end{aligned} \quad (3)$$

with

$$\sigma_H^2 = \Gamma(1-2H)\frac{\cos(\pi H)}{\pi H} \quad (4)$$

Eq. (3) shows that fractional Brownian motion is not a stationary process. Its samples have long-time correlations, theoretically extending till infinity. These facts make the analysis of *fBm* quite difficult. Even the problem of defining a spectral power density for a nonstationary process is not trivial. This problem was solved by P. Flandrin (Flandrin, 1989) who defined the spectral power density $S_{B_H}(\omega)$ as the time-average of the Wigner-Ville spectrum (the Fourier transform of the time-dependent autocorrelation function):

$$W_{B_H}(t,\omega) = \int_{-\infty}^{+\infty} R_{B_H}\left(t + \frac{\tau}{2}, t - \frac{\tau}{2}\right) e^{-j\omega\tau} d\tau \quad (5)$$

For large averaging intervals ($T \to \infty$), he obtained:

$$S_{B_H}(\omega) = \lim_{T\to\infty} \frac{1}{T}\int_0^T W_{B_H}(t,\omega)dt = \frac{1}{|\omega|^\gamma} \quad (6)$$

with $\gamma = 2H + 1$. This result is also valid for the n-dimensional *fBm* process (Voss, 1988; Saupe, 1988), with:

$$\gamma = 2H + n. \quad (7)$$

A simple method for the estimation of D is thus based on the computation of the power spectrum of the image. This power spectrum is represented in a log-log plot vs. frequency. According to eq. (6) the points of the plot will align along a line with slope $-\gamma$. The parameter γ is usually estimated via a regression technique and D is obtained from eqs. (7) and (2).

An alternative method for the estimation of D is based on the wavelet decomposition of *fBm* signals. Just like fractals, wavelets heavily rely on the scale concept, i.e. on the analysis of the data at several resolutions (Mallat, 1989; Wornell, 1993). Given a signal $x(t)$, a sequence $A_m x(t)$ of approximations $x(t)$ is constructed, each $A_m x(t)$ being specific for the representation of the signal at a given resolution (scale). Formally, the signal space V is decomposed into a nested sequence of approximation spaces:

$$\cdots \subset V_{-1} \subset V_0 \subset V_1 \subset V_2 \subset \cdots \quad (8)$$

and $A_m x(t)$ represents the projection of signal $x(t)$ from V onto subspace V_m so that this projection is the "closest" approximation of $x(t)$ with resolution 2^m. If we define

$$D_m x(t) = A_{m+1}x(t) - A_m x(t) \quad (9)$$

the detail signal at resolution 2^m, then this detail signal can be expressed as:

$$D_m x(t) = \sum_n x_n^m \psi_n^m(t) \quad (10)$$

with:

$$x_n^m = \int_{-\infty}^{\infty} x(t)\psi_n^m(t)dt \tag{11}$$

This equation is the *direct wavelet transform* of the signal $x(t)$. In the signal processing paradigm, it represents the expansion of $x(t)$ in the set of basis functions $\psi_n^m(t)$. These basis functions have a very special property: they are all dilations and translations of a single function $\psi(t)$ called *mother wavelet*:

$$\psi_n^m(t) = a_0^{m/2}\psi(a_0^m t - nb_0) \tag{12}$$

Usually, a particular choice of a_0 and b_0 is used: $a_0 = 2, b_0 = 1$. In this case, we obtain an orthonormal wavelet basis (Daubechies, 1992) with functions:

$$\psi_n^m(t) = 2^{m/2}\psi(2^m t - n) \tag{13}$$

The inverse discrete wavelet transform ("reconstruction formula") is given by:

$$x(t) = \sum_m \sum_n x_n^m \psi_n^m(t) \tag{14}$$

All given definitions and formulas can easily be extended from the 1-dimensional to the 2-dimensional case (Mallat, 1989). The wavelet transform describes thus at each resolution step the difference signal from the previous to the current resolution representation.

The similar fundamental concepts of the fractal and wavelet theory have stimulated several researchers to investigate this relation in more detail. The main result in this field is due to G. W. Wornell who showed that the wavelet transform applied to a *fBm* signal whitens the signal, i.e. the transformed-domain samples at a given resolution 2^m (the detail signal samples) become stationary and weakly correlated and both the theoretic and the numeric analysis are much easier to perform. The direct estimation of the fractal dimension relies in this case on the fact that the variance of the wavelet coefficients at level 2^m is given by:

$$\mathrm{Var}\, x_n^m = \sigma^2 2^{-\gamma m}, \qquad \sigma^2 > 0 \tag{15}$$

with σ^2 being a constant depending on the wavelet basis used, and γ given by eq. (7). Again, a log-log plot of $\mathrm{Var}\, x_n^m$ vs. resolution level m will yield a line with slope proportional to $-\gamma$. Alternatively, a maximum likelihood estimation algorithm (Wornell and Oppenheim, 1992) can be used to estimate γ.

3 COMPARISON OF FRACTAL MODELS

In order to compare the performance of the methods presented in the previous section, a set of 256-by-256 spatially isotropic *fBm* surfaces ranging from dimension 2.0 to dimension 3.0 was generated. In each image, the dimension was estimated locally in a sliding window of size 32-by-32 pixels with the spectral and the wavelet-based algorithm (using Daubechies wavelets with 4 filter coefficients).

One of the difficulties in the application of the wavelet-based analysis methods to images is the fact that these methods are essentially 1-dimensional. A 2-dimensional wavelet transform such as e.g. the one presented by Mallat in (Mallat, 1989) will not exhibit the specific standard deviation property (eq. 15) that constitutes the basis of the estimation algorithm. This problem has been solved by some authors by performing a 1-dimensional wavelet analysis for each row (column) in the sliding window and then averaging the obtained values (Kaplan and Kuo, 1994). The main disadvantage of this solution is the fact that only the square root of the total number of pixels in the window is used for the dimension estimation process. Since this process relies on statistical assumptions, it will lead to large errors in the case of small analysis windows. Additionally, no advantage is taken of the 2-dimensional image correlation, but only of the 1-dimensional statistics of the pixels.

To overcome these disadvantages, we have developed a different data organization method. The rows (columns) of the sliding window are scanned back and forth and then concatenated to form a single vector on which the estimation algorithm is applied (figure 1). In this way, all the data points are used for estimation and the scanning algorithm does not introduce discontinuities. The fractal dimension is estimated both in x and in y-direction and the two obtained values are averaged for each image point.

The comparison of the different estimation algorithms is performed by means of mainly two parameters: the "mean of measurements" and the "uniformity of measurements". These parameters are plotted vs. the real dimension of the fractal surface in figure 2. The mean of measurements represents the mean value of the fractal dimension estimations for all the positions of the sliding window. For a uniform surface of fractal dimension D, the mean $\hat{D}$ should yield the value $\hat{D} = D$, i.e. the ideal shape of the mean plot is that of the diagonal line. The uniformity of measurements is defined as the standard deviation of the measurements about the measured mean ($\hat{D}$). The uniformity plot should thus be flat and of minimal value to characterize a reliable estimation method.

The results of this analysis show that although the

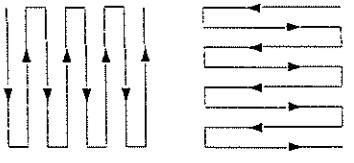

Figure 1: Scanning of the window used in the wavelet-based fractal dimension estimation

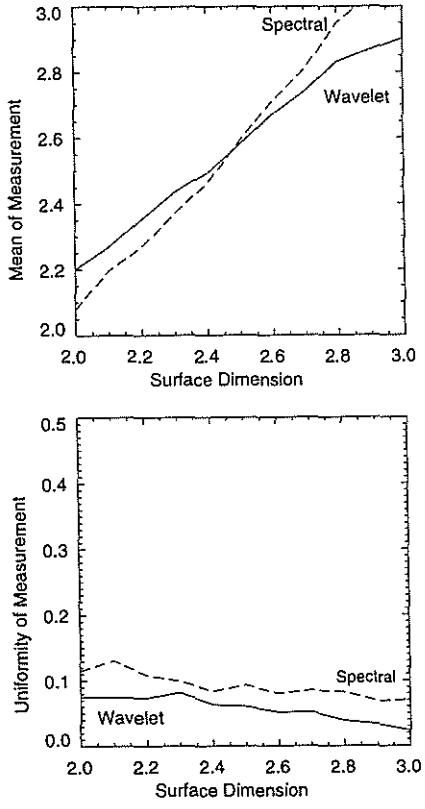

Figure 2: Mean and uniformity of fractal dimension measurements for synthetic surfaces. Window size = $32 \times 32 = 1024$ pixels

spectral method has a better performance in terms of measurement accuracy, the wavelet-based method has a substantially better uniformity. A good uniformity is in our opinion more important for image segmentation than the exact estimation of the numeric values for the fractal dimension, provided that the relation $\hat{D}$ vs. D remains monotonic. This is the case for the wavelet-based method, where the $\hat{D}$ vs. D plot can be used as a LUT for the correction of estimated values.

These results can be visualized by means of an example. Figure 3a shows a synthetic DEM (shown as a shaded relief) consisting of a central square of fractal dimension $D = 2.8$ surrounded by a rectangular border of fractal dimension $D = 2.2$. Figures 3b and c show the estimation results for D (i.e. for the roughness of the relief) using the spectral and the wavelet-based algorithms respectively in a sliding window of size 32×32 pixels. The estimated numeric values are scaled linearly from [2.0, 3.0] to [0, 255] and are presented as gray scale images. White corresponds to a high fractal dimension ("rough") and black to a low fractal dimension ("smooth"). To avoid problems generated by discontinuities on the borders of the image, we did not compute the fractal dimension in a swath of 16 pixels on each image side. This swath is shown here in black. Also note the smearing of the border of the central square: due to the large size of the sliding window, this smearing is significant and the square appears larger than in reality.

Figure 3 confirms the conclusions of the mean and uniformity plots. Due to the better uniformity of the wavelet-based estimation algorithm the fractal dimension map in figure 3b appears less noisy than the one computed with the spectral method (figure 3c). This leads to a better visual appearance and to an easier thresholding for segmentation.

4 APPLICATION TO DIGITAL ELEVATION MODELS

The algorithms described in the previous section have been tested on two elevation data sets that present different characteristics and allow us to consider different aspects of the fractal estimation process.

The first data set consists of three DEMs of the region of Davos, Switzerland at resolutions of 50m, 25m and 10m respectively (figure 4a). The DEMs were obtained by digitization of elevation data from maps of different resolution. For each of the DEMs the fractal dimension was computed in a sliding window of a size selected roughly proportional to the dimensions of the DEM (16×16 pixels for the 50m DEM, 32×32 pixels for the 25m DEM and 64×64 pixels for the 10m DEM).

Figure 4b shows the histograms of the estimated values for D obtained using the wavelet-based method. First note that all the histograms show a single peak. This fact means either that the whole considered area has a single fractal dimension or that it consists of several areas with very close fractal dimensions which cannot be differentiated by this method. Note also that the peak is at about the same position for all three histograms, i.e. the structure of the terrain is invariant to scale. Since the data of the three DEMs was obtained by independent processes and not by interpolation of one set to another, this example proves that the terrain shows indeed a fractal structure. The dimension of this fractal lies in the range of $D = 2.1$ to $D = 2.2$. Similar fractal dimension values have been reported for DEMs of other areas as well (Polidori et al., 1991; Clarke and Schweizer, 1991).

Figure 4c shows the histogram of the estimated values for D using the spectral method. The variance of the measurements is higher and the estimation of D is less reliable. This result confirms the simulations described in the previous section.

Our second example shows the possibility to use the estimation of fractal dimensions to detect artifacts in elevation data and to segment DEMs according to

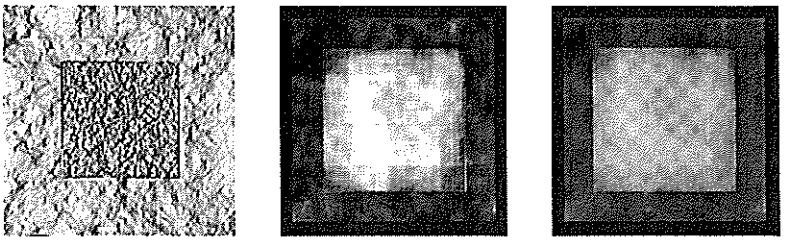

Figure 3: Segmentation example for synthetic DEM consisting of a central square of fractal dimension $D = 2.8$ surrounded by a border of fractal dimension $D = 2.2$. The dimension is estimated in a sliding window of size 32×32 pixels. a) Original image, b) Fractal dimension estimated with the spectral algorithm, c) Fractal dimension estimated with the wavelet-based algorithm

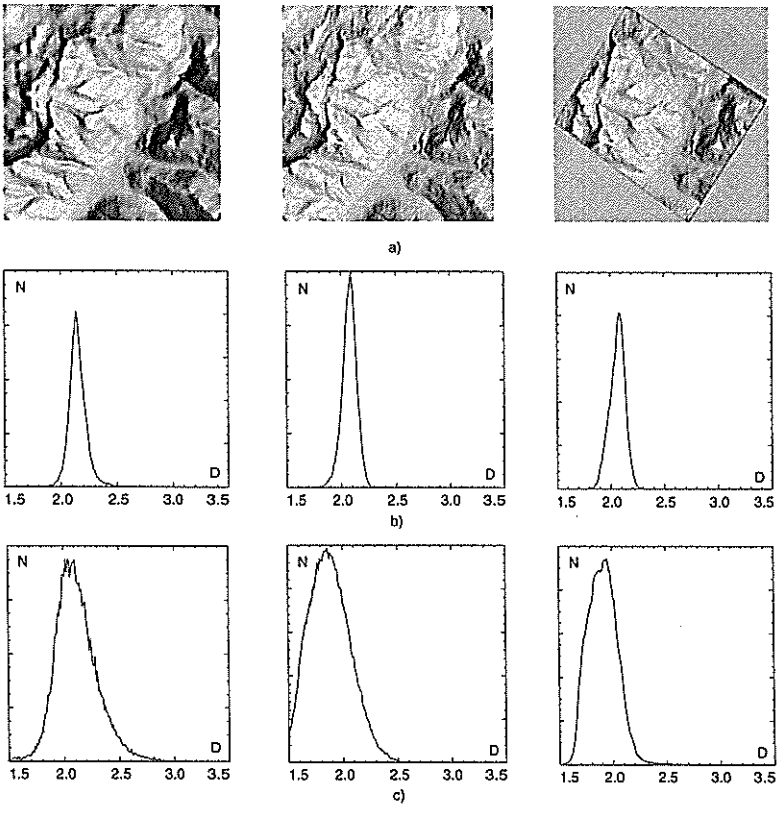

Figure 4: Fractal dimension measurements for three DEMs of different spatial resolution of the Davos area. a) DEMs presented as a shaded relief: left to right 50m, 25m, 10m; b) Histograms of fractal dimension measurements for the DEMs in figure a) using the wavelet-based method; c) Histograms of fractal dimension measurements for the DEMs in figure a) using the spectral method

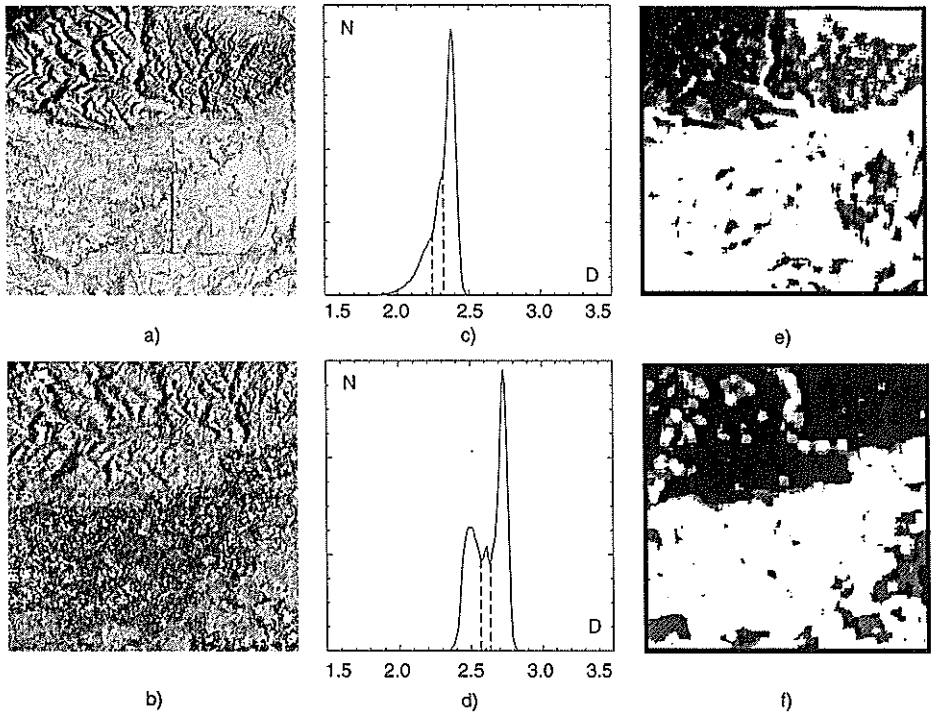

Figure 5: a) Topographic DEM of an area along the river Rhine; b) Interferometric DEM of approximately the same area; c) Histogram of fractal dimension measurements for the topographic DEM; d) Histogram of fractal dimension measurements for the interferometric DEM; e) Thresholded fractal dimension image for the topographic DEM; f) Thresholded fractal dimension image for the interferometric DEM

their roughness. The data consists of two DEMs of an area along the river Rhine in Germany. The first DEM (figure 5a) was obtained from digitized cartographic information and has a resolution of 25m, while the second one (figure 5b) was obtained by SAR interferometry and has a resolution of about 20m. Note also that the topographic DEM is represented in geographical coordinates and the interferometric DEM is shown in range/azimuth coordinates which are slightly rotated with respect to the geographical ones. In spite of these differences the data was not preprocessed (e.g. reinterpolated and rotated) since that would have affected the fractal structure of the images.

The topographic and the interferometric DEM were analysed by computing the fractal dimension in a sliding window of size 32×32 pixels. The histograms of the values for D obtained with the wavelet method are shown in figure 5c and d respectively. While for the topographic DEM, D lies in the range $2.0 \ldots 2.4$, the interferometric data has much higher fractal dimensions, ranging from 2.4 to 2.8. These values indicate that the interferometric method induces some artifacts leading to an unusually high roughness of the elevation data. The estimation of the fractal dimensions provides a good method to detect these artifacts in an automatic way.

Additionally, the histograms of D allow the segmentation of the DEMs according to their roughness. On both histograms three *modi* can be detected although on the histogram of the topographic image these *modi* partly overlap. The images can be segmented by setting thresholds at the separation borders between the *modi*, e.g. at the positions of the dotted lines in figures 5c and d. The result of this segmentation is shown in figure 5e and f. Three classes are obtained that correspond roughly to the three relief areas in the DEM: the mountain area (low roughness, shown as black), the plain area (high roughness, shown as white) and a transition area (medium roughness, shown as gray).

As a final experiment, another roughness measure, the standard deviation of the elevation values in an image window was computed for the topographic and the interferometric DEMs and compared to the fractal dimension. The result of this comparison is shown as a scatterogram of the values of σ vs. D (figure 6). Little correlation can be seen between the two roughness measures, especially in the case of the interferometric

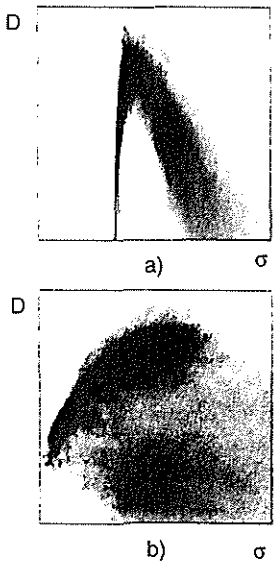

Figure 6: a) Scatterogram of the standard deviation of elevation data vs. fractal dimension for the topographic DEM b) Scatterogram of the standard deviation of elevation data vs. fractal dimension for the interferometric DEM

DEM where the points are scattered all over the plane $\sigma - D$. Obviously, the fractal dimension characterizes the roughness of the relief in a different way than the standard deviation of the elevation values. While σ is a parameter that assumes a Gaussian distribution, D relies on a fractional Brownian motion model which is non-Gaussian. The appropriateness of one of these measures is related to the assumptions that can be made on the statistics of the image.

5 CONCLUSIONS

The present paper compares some fractal methods for the characterization and segmentation of Digital Elevation Models. Based on important conceptual similarities between fractals and wavelets, we make the hypothesis that wavelets are a very appropriate analysis tools for fractal images. This assumption is confirmed by experiments both on simulated and on real elevation data: wavelet-based fractal dimension estimators show the highest reliability in terms of measurement variances and are thus better suited for DEM segmentation than other methods.

As an application we show some experiments on two DEMs of the same area: one obtained by map digitization and the other one by SAR interferometry. The DEMs can be easily segmented to several roughness classes by thresholding the histogram of the local fractal dimensions. Additionally, the fractal analysis of the elevation data can be used to identify some artifacts specific to the DEM derivation method: measurements on the interferometric DEM reveal that the data has an unusually high roughness due to typical interferometric artifacts.

6 ACKNOWLEDGEMENTS

We would like to acknowledge the German Remote Sensing Data Center (DFD) at DLR, Wessling, Germany for providing us the DEMs of the Rhine valley and the Remote Sensing Laboratories of the University of Zürich, Switzerland for providing us the 10m resolution DEM of the Davos area. Special thanks also to Dr. Marcus Schwäbisch from DLR for the derivation of the interferometric SAR DEM.

References

Akujuobi, C. M. and Baraniecki, A. Z. (1994). A comparative analysis of wavelets and fractals. In Leondes, C. T., editor, *Digital Image Processing: Techniques and Applications*, volume 67 of *Control and Dynamic Systems*, pages 143–197. Academic Press, Inc.

Clarke, K. C. (1988). Scale-based simulation of topographic relief. *The American Cartographer*, 15(2):173–181.

Clarke, K. C. and Schweizer, D. M. (1991). Measuring the fractal dimension of natural surfaces using a robust fractal estimator. *Cartography and Geographic Information Systems*, 18(1):37–47.

Daubechies, I. (1992). *Ten Lectures on Wavelets*. SIAM Press.

Flandrin, P. (1989). On the spectrum of fractional Brownian motions. *IEEE Trans. on Information Theory*, 35(1):197–199.

Franceschetti, G., Migliaccio, M., and Riccio, D. (1994). SAR simulation of natural landscapes. In Stein, T. I., editor, *Surface and Atmospheric Remote Sensing: Technologies, Data Analysis and Interpretation, IGARSS'94, Pasadena*, pages 1181–1183.

Huang, J. and Turcotte, D. L. (1990). Fractal image analysis: application to the topography of Oregon and synthetic images. *J. Opt. Soc Am. A*, 7(6):1124–1130.

Kaplan, L. M. and Kuo, C.-C. J. (1994). Fast fractal feature extraction for texture segmentation. In Chen, S.-S., editor, *Neural and Stochastic Methods in Image and Signal Processing III*, volume 2304, pages 144–155. SPIE.

Mallat, S. G. (1989). A theory for multiresolution signal decomposition: The wavelet representation. *IEEE Trans. on PAMI*, 11(7):674–693.

Mandelbrot, B. B. (1982). *The Fractal Geometry of Nature*. Freeman, CA.

Mandelbrot, B. B. and van Ness, J. W. (1968). Fractional Brownian motions, fractional noises and applications. *SIAM Review*, 10(4):422–437.

Polidori, L., Chorowicz, J., and Guillande, R. (1991). Description of terrain as a fractal surface, and application to digital elevation model quality assessment. *Photogrammetric Engineering & Remote Sensing*, 57(10):1329–1332.

Saupe, D. (1988). Algorithms for random fractals. In H.-O. Peitgen, D. S., editor, *The Science of Fractal Images*, chapter 2, pages 71–120. Springer-Verlag.

Schepers, H. E., van Beek, J. H. G. M., and Bassingtwaighte, J. B. (1992). Four methods to estimate the fractal dimension from self-affine signals. *IEEE Engineering in Medicine and Biology*, pages 57–71.

Stewart, C. V., Moghaddam, B., Hintz, K. J., and Novak, L. M. (1993). Fractional Brownian motion models for synthetic aperture radar imagery scene segmentation. *Proceedings of the IEEE*, 81(10):1511–1521.

Voss, R. F. (1988). Fractals in nature: From characterization to simulation. In Peitgen, H.-O. and Saupe, D., editors, *The Science of Fractal Images*, chapter 1, pages 21–70. Springer-Verlag.

Wornell, G. W. (1993). Wavelet-based representations for the $1/f$ family of fractal processes. *Proceedings of the IEEE*, 81(10):1428–1450.

Wornell, G. W. and Oppenheim, A. V. (1992). Estimation of fractal signals from noisy measurements using wavelets. *IEEE Trans. on Signal Processing*, 40(3):611–623.

Yokoya, N. and Yamamoto, K. (1989). Fractal-based analysis and interpolation of 3D natural surface shapes and their application to terrain modeling. *Computer Vision, Graphics and Image Processing*, 46:284–302.